Journal of Computational Physics **180,** 686–709 (2002)
doi:10.1006/jcph.2002.7112

A General Deterministic Treatment of Derivatives in Particle Methods

Jeff D. Eldredge,[1] Anthony Leonard, and Tim Colonius

Division of Engineering and Applied Science, California Institute of Technology, Pasadena, California 91125
E-mail: jde26@eng.cam.ac.uk, tony@galcit.caltech.edu, and colonius@caltech.edu

Received April 26, 2001; revised March 25, 2002

A unified approach to approximating spatial derivatives in particle methods using integral operators is presented. The approach is an extension of particle strength exchange, originally developed for treating the Laplacian in advection–diffusion problems. Kernels of high order of accuracy are constructed that can be used to approximate derivatives of any degree. A new treatment for computing derivatives near the edge of particle coverage is introduced, using "one-sided" integrals that only look for information where it is available. The use of these integral approximations in wave propagation applications is considered and their error is analyzed in this context using Fourier methods. Finally, simple tests are performed to demonstrate the characteristics of the treatment, including an assessment of the effects of particle dispersion, and their results are discussed.

Key Words: particle methods; numerical simulation; vortex methods.

1. INTRODUCTION

Particle-based Lagrangian numerical methods are useful for analyzing many different physical phenomena. The vortex particle method (VPM) has become a useful tool for computing incompressible flows in which vorticity is an integral component [5], and recently, the VPM has been adapted to compressible flows by Eldredge *et al.* [9]. The method of smoothed particle hydrodynamics (SPH) is applied in the contexts of astrophysical fluid dynamics and gas dynamics [11]. In each of these methods it is often necessary to compute derivatives of the primary variables. In viscous applications of the VPM, the governing equations contain the Laplacian of the vorticity. In SPH the gradient of the pressure is computed. The compressible VPM of Eldredge *et al.* [9] requires calculation of the Laplacian of the enthalpy, as well as gradients of enthalpy and entropy in the baroclinic term. The challenge in each of these methods lies in accurately

[1] Present address: Department of Engineering, Cambridge University, Cambridge CB2 1PZ, UK.

0021-9991/02 $35.00

computing the derivative of a quantity from information only available at scattered locations.

The developers of these methods have devised many different schemes for treating these derivatives. Although the methods have evolved independently, the schemes they use are largely based on the same principle, that particles are collaborative entities with global rather than local, isolated behavior, so it is natural to use cumulative (i.e., integral) operators to approximate local (i.e., differential) operators. For instance, SPH is based on the interpolation of a field quantity by a finite set of "smoothed particles"; the pressure gradient is computed by simply applying the gradient operator directly to the interpolation kernel [11]. The VPM shares the interpolative character with SPH: when the Biot–Savart kernel is mollified by a blob function, the singular vortex particles become regular vortex blobs. Thus, for her viscous VPM, Fishelov [10] used the same idea as in SPH, applying the differential operator directly to the blob function for computing the Laplacian of the vorticity.

Particle strength exchange, or PSE, was developed from a different approach. Earlier work by Choquin and Huberson [1] and Cottet and Mas-Gallic [7] involved a viscous splitting of the Navier–Stokes equations, with the diffusive component solved by means of a convolution with the heat kernel. When manipulated into a conservative form, Mas-Gallic and Raviart [13] found that this diffusion treatment revealed a larger class of schemes that allowed kernels other than the heat kernel. Degond and Mas-Gallic [8] developed the method in greater detail and presented a treatment for general convection–diffusion problems. They first approximate the Laplacian by an integral operator and then discretize the integral by a quadrature over the particles. Their techniques is now commonly known as PSE because of the conservation properties that are inherent when two particles "exchange strength" with one another. This conservation property is particularly important, as the decay (or growth) of a supposedly invariant global quantity can seriously degrade the accuracy of a computation. Conservation is not unique to PSE: with a slight modification the SPH formula can be made to conserve linear and angular momentum [11]. The method of Fishelov [10] is approximately conservative to the degree of accuracy of the quadrature, which under some conditions, discussed in Section 3, is spectral. The symmetry of PSE, however, provides it with natural and exact conservativeness.

Particle strength exchange has been used extensively in vortex methods. The accuracy of the approach was explored by Choquin and Lucquin-Desreux [2] on model problems and compared with that of the random walk method. Winckelmans and Leonard [16] used the technique to account for viscous diffusion in three-dimensional simulations of vortex rings. Koumoutsakos *et al.* [12] used it in conjunction with a wall flux treatment in their development of boundary conditions for viscous vortex methods. Ploumhans and Winckelmans [15] adapted the method to account for particles of different core sizes and developed an image treatment near walls to remove spurious vorticity flux.

In the present work we show that the framework used to develop PSE and its kernel can be generalized to approximate arbitrary spatial differential operators in many different physical contexts. It should be noted that the approaches used in [10, 11] also allow for generalization. We concentrate on PSE because of the exact conservation that it naturally provides. In addition, we extend the full-space operators to "one-sided" operators, useful in configurations where particle coverage is asymmetric, such as near boundaries. Furthermore, we present an analysis of the error of these integral operators in the context of wave convection. Finally, we demonstrate the use of these approximate operators on several model problems and discuss the results.

2. PARTICLE STRENGTH EXCHANGE

In a particle method, the computational elements are particles, transported by the local velocity field. The instantaneous location of particle p, $\mathbf{x}_p(t)$, is given by the flow map, $\mathbf{x}_p(t) = \mathbf{X}(t; \xi_p)$, where ξ_p is the particle's initial location and the flow map is derived from the integration of the velocity field, $\mathbf{u}$. Thus, the particle location is governed by

$$\begin{aligned} \frac{d\mathbf{x}_p}{dt} &= \mathbf{u}(\mathbf{x}_p(t), t), \\ \mathbf{x}_p(0) &= \xi_p. \end{aligned}$$

The value of a field quantity, f, at $\mathbf{x} = \mathbf{x}_p(t)$ is identified with a particle strength per unit volume, $f_p(t)$, and the field is composed of the collection of particles

$$f(\mathbf{x}, t) = \sum_p V_p(t) f_p(t) \zeta_\varepsilon(\mathbf{x} - \mathbf{x}_p(t)),$$

where V_p is the particle volume and ζ_ε is a regularized function that approaches a Dirac measure as its radius, ε, goes to zero. The particle volume changes according to the divergence of the velocity field,

$$\frac{dV_p}{dt} = \operatorname{div} \mathbf{u}(\mathbf{x}_p(t), t) V_p(t).$$

For differential operators we use the notation

$$D^\beta = \frac{\partial^{|\beta|}}{\partial x_1^{\beta_1} \partial x_2^{\beta_2} \dots \partial x_d^{\beta_d}},$$

where $\beta = (\beta_1, \beta_2, \dots, \beta_d)$ is a multiindex, $|\beta| \equiv \beta_1 + \beta_2 + \cdots + \beta_d$, and d is the physical dimension. Also, $\mathbf{y}^\beta = y_1^{\beta_1} y_2^{\beta_2} \dots y_d^{\beta_d}$ and $\beta! = \beta_1! \beta_2! \dots \beta_d!$. A sum

$$\sum_{|\beta|=1}^{\infty}$$

denotes a double sum, an inner sum over all multiindices β with sum equal to $|\beta|$, and an outer sum over all values of $|\beta| \geq 1$.

The general integral PSE operator for approximating the action of D^β on f has the form

$$L^\beta f(\mathbf{x}) = \frac{1}{\varepsilon^{|\beta|}} \int (f(\mathbf{y}) \mp f(\mathbf{x})) \eta_\varepsilon^\beta(\mathbf{x} - \mathbf{y}) \, d\mathbf{y}, \tag{1}$$

where η^β is the kernel and $\eta_\varepsilon(\mathbf{x}) = \eta(\mathbf{x}/\varepsilon)/\varepsilon^d$, where ε is the kernel radius. For conservation reasons, to be discussed shortly, the sign chosen for the term in parentheses depends on whether $|\beta|$ is even or odd. If even, then the negative sign is chosen, and if odd, the positive sign is used. The integral is discretized by midpoint quadrature over the particles, resulting in the following operator:

$$L_h^\beta(t) f_p = \frac{1}{\varepsilon^{|\beta|}} \sum_q V_q(t) (f_q(t) \mp f_p(t)) \eta_\varepsilon^\beta(\mathbf{x} - \mathbf{x}_q(t)). \tag{2}$$

From here on, the time dependence of the quantities will not be explicitly written except to avoid ambiguity.

The rationale for the "strength exchange" label becomes clear if we consider the application to specific equations. For example, on application of (2) to the Laplacian operator in the convection–diffusion equation, the particle strengths evolve according to

$$\frac{dF_p}{dt} = \frac{1}{\varepsilon^2} \sum_q (V_p F_q - V_q F_p) \eta_\varepsilon^{\text{lap}}(\mathbf{x}_p - \mathbf{x}_q), \tag{3}$$

where $F_p \equiv V_p f_p$ and the superscript of η denotes its use for the Laplacian. For reasons explained in the next section, the kernel for this operator is constructed to be even in both coordinate directions. Thus, the right-hand side has a skew symmetry such that when the equation is integrated, the portion of strength lost by particle p in its interaction with q will be exactly equal to the portion gained by q. If both sides of (3) are summed over all the particles, the right-hand side cancels identically and thus the total strength is conserved. If the equation considered had instead a first derivative, then the kernel should be odd in its argument, and conservation would be guaranteed if the strengths in the summand were added rather than subtracted.

3. METHODOLOGY

The derivation of formula (1) is not restricted to the Laplacian operator. In fact, *any* differential operator can be given an integral approximation of *any* order of accuracy, provided the kernel obeys the appropriate set of moment conditions.

3.1. Full-Space Integral Approximations

Consider a Taylor expansion of the function, f, about a point $\mathbf{x}$ and evaluate the expansion at another point, $\mathbf{y}$:

$$f(\mathbf{y}) = f(\mathbf{x}) + \sum_{|\alpha|=1}^{\infty} \frac{1}{\alpha!} (\mathbf{y} - \mathbf{x})^\alpha D^\alpha f(\mathbf{x}). \tag{4}$$

Now $f(x)$ is subtracted from both sides and each term is convolved with the unknown kernel η^β scaled by ε. The result is

$$\varepsilon^{|\beta|} L^\beta f(\mathbf{x}) = \sum_{|\alpha|=1}^{\infty} \frac{1}{\alpha!} D^\alpha f(\mathbf{x}) \int (\mathbf{y} - \mathbf{x})^\alpha \eta_\varepsilon^\beta (\mathbf{x} - \mathbf{y})\, d\mathbf{y},$$

where the operator L^β is defined in Eq. (1), with the negative sign chosen. The variables of integration are translated and rescaled to simplify the integrals to

$$L^\beta f(\mathbf{x}) = \sum_{|\alpha|=1}^{\infty} \frac{(-1)^{|\alpha|} \varepsilon^{|\alpha|-|\beta|}}{\alpha!} D^\alpha f(\mathbf{x}) M_\alpha, \tag{5}$$

where for notational simplicity the α-moment has been defined as

$$M_\alpha = \int \mathbf{y}^\alpha \eta(\mathbf{y})\, d\mathbf{y}. \tag{6}$$

Now the derivative that will be approximated is isolated on the right-hand side. A linear combination of derivatives can also be approximated, of course, but only one is considered here:

$$L^\beta f(\mathbf{x}) = \frac{(-1)^{|\beta|}}{\beta!} M_\beta D^\beta f(\mathbf{x}) + \sum_{\substack{|\alpha|=1 \\ |\alpha|\neq|\beta|}}^{\infty} \frac{(-1)^{|\alpha|}}{\alpha!} \varepsilon^{|\alpha|-|\beta|} M_\alpha D^\alpha f(\mathbf{x}) + \sum_{\substack{|\alpha|=|\beta| \\ \alpha\neq\beta}} \frac{(-1)^{|\beta|}}{\alpha!} M_\alpha D^\alpha f(\mathbf{x}). \tag{7}$$

To construct a useful approximation, the moments that appear inside the summations on the right-hand side must vanish to some degree and the β-moment must be nonzero. With these goals in mind, for an approximation of order r, a set of moment conditions,

$$M_\alpha = \begin{cases} (-1)^{|\beta|}\beta!, & \alpha = \beta, \\ 0, & |\alpha| = |\beta|,\ \alpha \neq \beta, \\ 0, & |\alpha| \in [1, |\beta| - 1] \cup [|\beta| + 1, |\beta| + r - 1], \end{cases} \tag{8}$$

as well as

$$\int |\mathbf{y}|^{|\beta|+r} |\eta^\beta(\mathbf{y})|\, d\mathbf{y} < \infty, \tag{9}$$

is imposed.

Provided these conditions are satisfied, the error in approximating the differential operator by (1) is bounded by (see[8])

$$\| D^\beta f - L^\beta f \|_{0,2} \leq C_1 \varepsilon^r \| f \|_{r+2,2}, \tag{10}$$

where C_1 is some constant and $\| \cdot \|_{k,m}$ is the norm of the $W^{k,m}(\mathbb{R}^d)$ Sobolev space. The quadrature approximation of the integral operator incurs additional error, which is bounded by

$$\| L^\beta f - L_h^\beta(t) f \|_{0,2} \leq C_2 \frac{h^m}{\varepsilon^{m+|\beta|-1}} \| f \|_{m,2}, \tag{11}$$

provided that $\eta \in W^{m,1}(\mathbb{R}^d)$, $f \in W^{m,2}(\mathbb{R}^d)$, and the flow map is smooth. Thus, the error bound accounts for distortion in the particle grid, but it should be noted that the proportionality constant, C_2, is dependent upon the duration of the simulation and the velocity field to which the particles are subjected. In practice it is found that the particles must occasionally be reinitialized to control dispersion that tends to degrade the quadrature.

Gaussian kernels such as those considered below belong to $W^{\infty,1}(\mathbb{R}^d)$, which appears to make the quadrature spectrally accurate, provided that $\varepsilon > h$. In fact, when the domain is finite, the proof of the error estimate also assumes either that the function f is periodic or that the function and its derivatives vanish on the boundary of the domain. It is well-known that midpoint quadrature leads to superb accuracy under these conditions, but if these do not hold, then the estimate reverts to second order. However, reducing the error in (10) through

an increase in the order of accuracy, r, is still very effective at mitigating the overall error, as the examples in Section 5 will show.

The construction of the kernel is simplified considerably if we assume some symmetry in its form. For instance, if the derivative we wish to approximate is even in the x_l-direction (i.e., β_l is even), then we will construct $\eta^\beta(\mathbf{x})$ to be even with respect to this direction, and consequently all moments in (8) for which α_l is odd automatically vanish. Similarly, if β_l is odd, then $\eta^\beta(\mathbf{x})$ should be odd in this direction. With this symmetry,

$$\eta^\beta(-\mathbf{x}) = (-1)^{|\beta|}\eta^\beta(\mathbf{x}). \tag{12}$$

With this form of kernel, the integral PSE operator (1) can take either sign in the integrand when $|\beta|$ is odd with no effect on its accuracy: the operator resulting from the Taylor expansion above can be expressed as

$$L^\beta f = \frac{1}{\varepsilon^{|\beta|}}\left(\eta_\varepsilon^\beta \star f - M_0 f\right),$$

where $\star$ denotes convolution. The second term is zero if $|\beta|$ is odd because the zeroth moment vanishes. Thus, the subtraction may be replaced by addition without affecting the approximation. However, the discretized operator (2) retains both terms because of the conservation that it allows. The choice of sign is made because of (12).

Some examples will serve to illustrate the procedure of constructing a kernel. Consider the original intent of the formula, to approximate the Laplacian operator. A kernel of order $r = 2$ will be constructed for two-dimensional applications. In this case, the differential operator is $\nabla^2 = D^{(2,0)} + D^{(0,2)}$, and the moment conditions are

$$\begin{aligned} &M_{(1,0)} = 0, \quad M_{(0,1)} = 0, \\ &M_{(2,0)} = 2, \quad M_{(1,1)} = 0, \quad M_{(0,2)} = 2. \end{aligned} \tag{13}$$

At first sight, it looks as though the kernel would need 5 degrees of freedom to satisfy the entire set of five conditions. However, if the form of the kernel is chosen carefully, then many of these conditions are redundant. For instance, choose the template

$$\eta(\mathbf{x}) = \frac{1}{\pi}\left(\sum_{j=0}^{m} \gamma_j |\mathbf{x}|^{2j}\right) e^{-|\mathbf{x}|^2}. \tag{14}$$

The kernel possesses the symmetric form discussed above, so all of the moments with at least one odd index vanish immediately without consideration of the coefficients, γ_j. Also, it can be shown that all of the remaining conditions for a given value of $|\alpha|$ (i.e., on a given row in the moment table (13)) are satisfied if one of the conditions is satisfied (including the $M_{(2,0)}$ and $M_{(0,2)}$ conditions, due to the symmetry of the kernel). Thus, only *one* coefficient is needed to satisfy five conditions. The reason for this reduction is that the conditions were expressed in Cartesian coordinates, whereas a cylindrical system would be more appropriate for this particular operator. In fact, for a kernel of order r, we would need only $r/2$ coefficients (i.e., $m = r/2 - 1$). Upon substituting the template (14) into (6) and then expressing the integral in the more natural cylindrical system, each moment becomes

a linear combination of the coefficients, γ_j,

$$M_\alpha = \frac{1}{\pi}\frac{\Gamma\left(\frac{\alpha_1+1}{2}\right)\Gamma\left(\frac{\alpha_2+1}{2}\right)}{\Gamma\left(1+\frac{|\alpha|}{2}\right)}\sum_{j=0}^{r/2-1}\gamma_j\Gamma\left(j+1+\frac{|\alpha|}{2}\right), \tag{15}$$

where Γ is the gamma function. Continuing with the $r=2$ example, an algebraic equation is formed for the coefficient,

$$\frac{1}{\pi}\Gamma(3/2)\Gamma(1/2)\gamma_0 = 2,$$

and the resulting kernel is $\eta^{\text{lap}}(\mathbf{x}) = \frac{4}{\pi}e^{-|\mathbf{x}|^2}$.

Now we derive a fourth-order-accurate kernel for application to first derivatives in two-dimensional problems. Derivatives in the x_1-direction are considered, but adaptation to the other direction is straightforward. The moments conditions are

$$\begin{aligned}
&M_{(1,0)} = -1, \quad M_{(0,1)} = 0, \\
&M_{(2,0)} = 0, \quad M_{(1,1)} = 0, \quad M_{(0,2)} = 0, \\
&M_{(3,0)} = 0, \quad M_{(2,1)} = 0, \quad M_{(1,2)} = 0, \quad M_{(0,3)} = 0, \\
&M_{(4,0)} = 0 \quad M_{(3,1)} = 0, \quad M_{(2,2)} = 0, \quad M_{(1,3)} = 0, \quad M_{(0,4)} = 0.
\end{aligned} \tag{16}$$

Again, many of these conditions are redundant if we choose our kernel template wisely. We use

$$\eta(\mathbf{x}) = \frac{x_1}{\pi}\left(\sum_{j=0}^{m}\gamma_j|\mathbf{x}|^{2j}\right)e^{-|\mathbf{x}|^2}, \tag{17}$$

for which all of the moments with at least one even index vanish, and in fact $m = r/2-1$ once again. The moments are then

$$M_\alpha = \frac{1}{\pi}\Gamma\left(\frac{\alpha_1+2}{2}\right)\Gamma\left(\frac{\alpha_2+1}{2}\right)\sum_{j=0}^{r/2-1}\gamma_j\frac{\Gamma\left(\frac{2j+|\alpha|+3}{2}\right)}{\Gamma\left(\frac{|\alpha|+3}{2}\right)}. \tag{18}$$

For the present example, only two coefficients are needed to satisfy 14 conditions. The set of algebraic equations for the two coefficients is

$$\begin{bmatrix}\Gamma(2) & \Gamma(3)\\ \Gamma(3) & \Gamma(4)\end{bmatrix}\begin{pmatrix}\gamma_0\\ \gamma_1\end{pmatrix} = \begin{pmatrix}-2\Gamma(2)\\ 0\end{pmatrix}.$$

The resulting kernel is $\eta^{(1,0)}(\mathbf{x}) = \frac{x_1}{\pi}(-6+2|\mathbf{x}|^2)e^{-|\mathbf{x}|^2}$; for derivatives in the other direction, the factor x_1 need only be replaced by x_2. The Appendix contains a list of kernels of several orders of accuracy for many applications in both one and two space dimensions.

3.2. One-Sided Integral Approximations

In some circumstances, it is useful to have integral approximations that are "one-sided." In other words, the integration proceeds only over a half-space, with the particle defining

the local origin. In this way, a particle only interacts with particles in this half-space, and more precisely, only with particles in the intersection of this half-space with the kernel support. This is particularly useful near boundaries, where particles only have a partial set of neighbors.

A "left-sided" integral operator L_L^β is defined as

$$L_L^\beta f(\mathbf{x}) = \frac{1}{\varepsilon^{|\beta|}} \int_{\Omega^L} (f(\mathbf{y}) - f(\mathbf{x}))\eta_\varepsilon^{L,\beta}(\mathbf{x}-\mathbf{y})\, d\mathbf{y}, \tag{19}$$

where the integration is over the half-space defined as $\Omega^L = \{(y_1, y_2, \ldots, y_d) \in \mathbb{R}^d | y_1 \le x_1\}$ (i.e., the left-half space). Similarly, a "right-sided" operator is integrated over $\Omega^R = \{(y_1, y_2, \ldots, y_d) \in \mathbb{R}^d | y_1 \ge x_1\}$. Note that there is no choice to make about the sign in the integrand as there was in the full-space case, because these operators lack the symmetry to conserve strength. The discrete form of the left-sided operator is

$$L_{L,h}^\beta f_p = \frac{1}{\varepsilon^{|\beta|}} \sum_{\substack{q \\ \mathbf{x}_q \in \Omega^L}} V_q (f_q - f_p)\eta_\varepsilon^{L,\beta}(\mathbf{x}_p - \mathbf{x}_q). \tag{20}$$

This special treatment does not change the derivation of the last section significantly. We define a right-sided moment of the kernel as

$$M_\alpha^R = \int_{-\infty}^{\infty}\int_{-\infty}^{\infty}\cdots\int_{0}^{\infty} \mathbf{y}^\alpha \eta^L(\mathbf{y})\, dy_1\, dy_2 \ldots dy_d, \tag{21}$$

subject to the same conditions (8)–(9) as before. A right-sided moment appears in the derivation of the left-sided operator because when the integrals are expressed in the local particle-centered coordinate system, convolution uses a reflected form of the kernel and thus swaps the limits of integration. However, it should be noted that if the same symmetry form is assumed for one-sided kernels as for full-space ones, then the right- and left-sided moments are related very simply: $M_\alpha^R = (-1)^{|\alpha|-|\beta|} M_\alpha^L$. In particular, $M_\beta^R = M_\beta^L$, and since all other moments are constrained to be zero, *kernels derived for left-sided PSE operators can also be used in right-sided operators, and vice versa*.

We derive here a second-order left-sided kernel for approximating $\frac{\partial}{\partial x_1}$ in two dimensions. The same kernel template (17) will be used, although the kernel's oddness in the x_1-direction cannot be exploited, as in the full-space case, because of the new limits of integration in (21). The set of moment conditions is

$$\begin{aligned} &M_{(1,0)}^R = -1, \quad M_{(0,1)}^R = 0, \\ &M_{(2,0)}^R = 0, \qquad M_{(1,1)}^R = 0, \quad M_{(0,2)}^R = 0, \end{aligned} \tag{22}$$

and because the kernel is even in the x_2-direction, the moments with an odd second index are identically zero. Also, for the same reasons as in the full-space case, the rows on which all moments are constrained to be zero collapse to one condition. We thus need only two coefficients to satisfy the five conditions. The moments have analytical expression (cf., Eq. (18))

$$M_\alpha^R = \frac{1}{2\pi} \frac{\Gamma\left(\frac{\alpha_1+2}{2}\right)\Gamma\left(\frac{\alpha_2+1}{2}\right)}{\Gamma\left(\frac{|\alpha|+3}{2}\right)} \sum_{j=0}^{m} \gamma_j \Gamma\left(j + \frac{|\alpha|+3}{2}\right), \tag{23}$$

which are assigned the appropriate values to form two equations for the coefficients. Proceeding in this way we find that the second-order left-sided kernel is $\eta^{L,(1,0)}(\mathbf{x}) = \frac{x_1}{\pi}(-20 + 8|\mathbf{x}|^2)e^{-|\mathbf{x}|^2}$. Again, the same kernel can be used in a right-sided PSE operator, as well as for one-sided derivatives in the x_2-direction by replacing the x_1 factor.

3.3. Stability

Degond and Mas-Gallic [8] showed that the solution of the convection–diffusion equation with the diffusion operator replaced by its integral PSE counterpart is stable, provided certain conditions are satisfied. They offer two proofs of this stability: one requires that $\nu < C_s\varepsilon^2$, where ν is the diffusivity and C_s is a positive constant, and the other supposes that η is nonnegative. The first proof precludes the limit of vanishing ε for a given diffusivity, an unacceptable restriction. The second proof, which is termed "uniform stability," imposes no restriction on ε but limits the method to second-order accuracy, as only second-order-accurate kernels can be nonnegative. Cortez [3] avoids both of these constraints with a proof that merely requires that the Fourier transform of η satisfies $\hat{\eta}(\mathbf{k}) \leq \hat{\eta}(0)$. While kernels of greater than second order listed in the Appendix have negative portions, all the kernels listed have Fourier transforms that obey this constraint. Thus stability is guaranteed even for high-order-accurate kernels in convection–diffusion problems. When applied in other contexts (e.g., wave propagation), PSE should obey a similar bound.

The stability of the quadrature (2) relies on the condition that the ratio of kernel radius to interparticle spacing, $\kappa = \varepsilon/h$, be greater than unity (i.e., the kernels of neighboring particles must overlap). Without overlap, the particles cannot communicate and thus strength exchange breaks down. As time progresses the flow will distort the particle grid, and locally this overlap criterion may fail. As discussed above, it is important to reinitialize the particles occasionally. Some examples in Section 5 will clarify the importance of this remeshing.

The time discretization of an equation in which PSE is used carries further stability restrictions. While the proof of Degond and Mas-Gallic [8] for PSE applied to a convection–diffusion equation with forward Euler differencing in time relies on the assumption that the kernels are nonnegative, this is only a sufficient condition, and high-order-accurate kernels are likely to allow stable time differencing. Without proof, we posit that an upper limit on the time-step size of the problem is necessary for stability, as in conventional finite-difference schemes, except that the kernel radius, ε, is the relevant length scale rather than the interparticle spacing. For instance, in a diffusion problem with diffusivity ν, it is required that $\Delta t < C_d\varepsilon^2/\nu$, where C_d is some constant near unity, and in a convection problem, the "CFL" number is restricted, $\Delta t < C_c\varepsilon/c_0$, where c_0 is a typical wave speed. The constants will obviously depend on the time integration scheme used.

4. FOURIER ANALYSIS OF THE ERROR

The original intent of the PSE method was for application to convection–diffusion equations. When applied in such a parabolic context, the approximation modifies the original differential equation by adding diffusive error terms. The strength of this diffusion is related to the order of accuracy of the kernel. The application of PSE in this paper is extended to many different settings, including those involving wave propagation. In this setting, the role of the extra terms in the modified equation is *dispersive* rather than *diffusive*. As a

demonstration of this effect, consider the one-dimensional linear wave equation:

$$\frac{\partial^2 f}{\partial t^2} - \frac{\partial^2 f}{\partial x^2} = 0.$$

This equation is satisfied by a traveling wave, $e^{i(kx-\omega t)}$, for which the frequency is related to the wavenumber by $\omega(k) = \pm k$, indicating that it travels either to the left or the right at unit speed, regardless of the wavenumber. If the spatial derivative is approximated by a full-space PSE integral, the dependence of the frequency on the wavenumber for solutions of the modified equation is changed. The local slope of this dispersion relation for some wavenumber k is the group velocity of energy associated with k. Thus, a packet of waves with wavenumbers centered at k will propagate at this speed, and if this speed varies with k, then waves of larger bandwidth will be dispersed.

Here we explore this PSE-modified dispersion relation:

$$\frac{\partial^2 f}{\partial t^2} - \frac{1}{\varepsilon^2} \int_{-\infty}^{\infty} (f(y) - f(x)) \eta_\varepsilon^{(2)}(x-y)\, dy = 0.$$

Substitute the representative waveform $f(x,t) = e^{i(kx-\omega t)}$ and simplify to get

$$\omega^2 = \frac{1}{\varepsilon^2}\left(M_0 - \hat{\eta}^{(2)}(\varepsilon k)\right),$$

where $\hat{\eta}$ denotes the Fourier transform of the kernel and M_0 is the zeroth moment. Thus, for the traveling wave to be a solution to the modified equation,

$$\omega(k) = \pm \frac{1}{\varepsilon} \sqrt{M_0 - \hat{\eta}^{(2)}(\varepsilon k)}.$$

With respect to the exact relation, the right-hand side can be regarded as a modified wavenumber, $k_{mod}(k)$:

$$k_{mod}(k) = \frac{1}{\varepsilon} \sqrt{M_0 - \hat{\eta}^{(2)}(\varepsilon k)}. \tag{24}$$

Expanding $\hat{\eta}^{(2)}(\varepsilon k)$ in a Taylor series about $\varepsilon k = 0$, and assuming that the rth-order-accurate kernel is symmetric with respect to x, the modified wave number can be written as

$$\begin{aligned} k_{mod}(k) &= k \left[1 + \sum_{n=r/2+1}^{\infty} \frac{(\varepsilon k)^{2(n-1)}(-1)^{n-1}}{(2n)!} M_{2n} \right]^{1/2} \\ &\approx k \left(1 + \frac{1}{2} \sum_{n=r/2+1}^{\infty} \frac{(\varepsilon k)^{2(n-1)}(-1)^{n-1}}{(2n)!} M_{2n} \right). \end{aligned} \tag{25}$$

Thus, the wavenumber is modified by the second term in parentheses. This term is dependent upon k, so the speed of a traveling wave will depend upon k as well and thus the PSE approximation is dispersive. However, increasing the order of accuracy of η clearly reduces the strength of this dispersion, as the leading-order modification of the wave number is proportional to ε^r.

We have so far only considered the dispersive effects of the integral PSE approximation, but in practice we use a discretized form of this. The discrete analog of (24) is

$$k_{mod}(k) = \frac{1}{\varepsilon}\sqrt{\tilde{M}_0 - \tilde{\eta}^{(2)}(k)}, \tag{26}$$

where $\tilde{M}_0$ is the discrete zeroth moment,

$$\tilde{M}_0 = \frac{h}{\varepsilon}\sum_{p=-\infty}^{\infty} \eta^{(2)}(ph/\varepsilon), \tag{27}$$

and $\tilde{\eta}^{(2)}$ is the discrete Fourier transform of the kernel,

$$\tilde{\eta}(k) = \frac{h}{\varepsilon}\sum_{p=-\infty}^{\infty} e^{ikph}\eta^{(2)}(ph/\varepsilon). \tag{28}$$

We have assumed here a grid of infinite extent with spacing h, which is a reasonable approximation to an actual grid of finite length, provided that in the latter we consider the solution away from the ends of the grid.

Figure 1a depicts the modified wavenumber—computed numerically—for the discrete PSE operator using kernels of various orders of accuracy. According to the Nyquist sampling theorem, the maximum wavenumber we can resolve on this grid is π/h. When the data of nearby particles varies on a spatial scale that approaches the interparticle spacing, the wavenumber content of the data extends to π/h. For the second-order-accurate kernel, the group velocity, dk_{mod}/dk, strays from unity even for small wavenumbers. However, increasing the order of accuracy of the PSE kernel has a considerable effect on its approximating ability. The eighth-order-accurate PSE scheme is much less dispersive.

A similar analysis can be performed for the first-derivative PSE operator in the context of the one-dimensional convection equation,

$$\frac{\partial f}{\partial t} + \frac{\partial f}{\partial x} = 0.$$

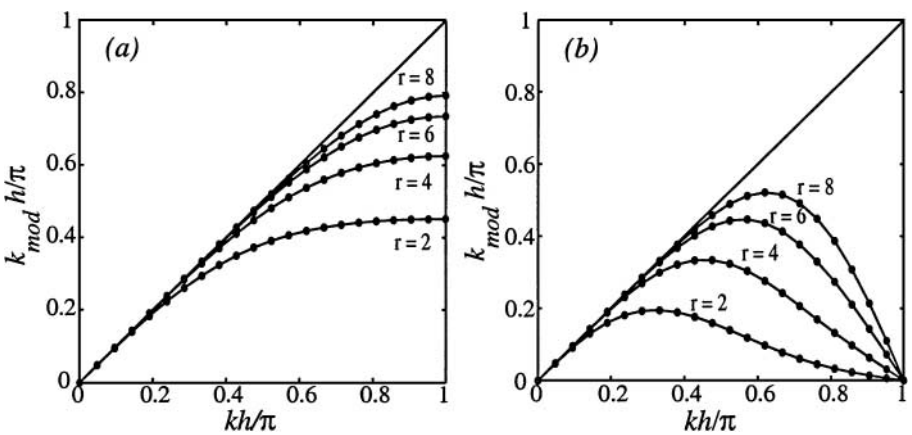

FIG. 1. Modified wavenumber in applying PSE to (a) wave equation and (b) first-order convection equation, with second-, fourth-, sixth-, and eighth-order kernels; $\kappa = 1.4$. Exact, ———; discrete PSE, —○—.

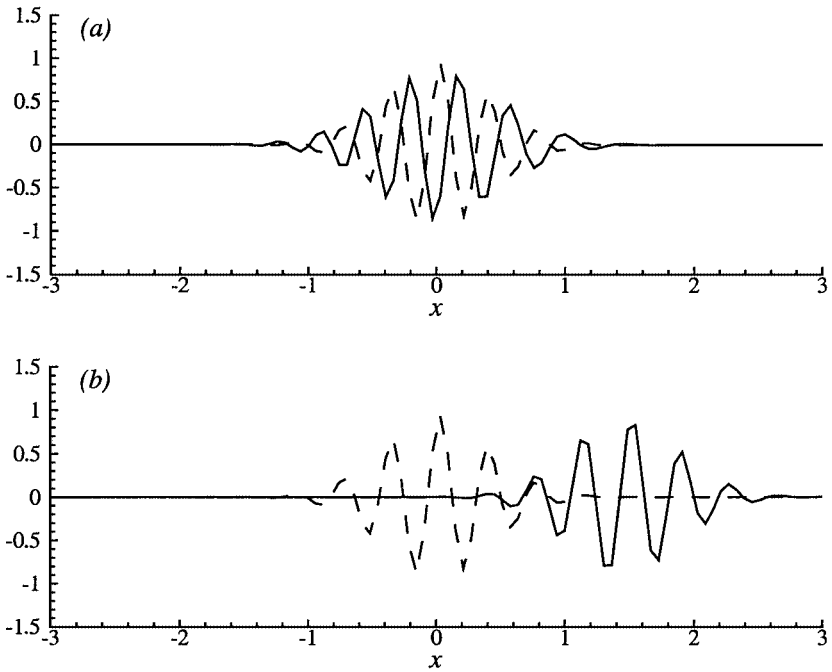

FIG. 2. Packet of waves centered at $k_0 = 0.32\pi/h$, convected with (a) second-order and (b) eighth-order PSE. At $t = 0$, – – –; at $t = 1.5$, ——.

Assuming the same form of solution as before, the frequency and wavenumber are found to be related by $\omega(k) = k$, so waves of any wavenumber travel with unit speed in the positive x-direction. The modified wavenumber using the discrete PSE operator for the first derivative can be shown to be

$$k_{mod}(k) = -\frac{i}{\varepsilon}\tilde{\eta}^{(1)}(k). \tag{29}$$

This relation is plotted in Fig. 1b for $r = 2$, 4, 6, and 8. The same poor behavior of the low-order-accurate PSE operators is apparent, as is the significant improvement using higher-order-accurate kernels. Figure 2a demonstrates the importance of minimizing dispersion. A packet of waves of the form

$$f(x) = \frac{1}{\sqrt{\pi\sigma^2}} e^{-(x-x_0)^2/\sigma^2} \cos(k_0 x),$$

with radius $\sigma = 0.1$, is used as an initial condition for the convection equation, to which a second-order PSE approximation is applied. The packet is Gaussian distributed about the wavenumber k_0, which we set to $0.32\pi/h$. According to Fig. 1b, the PSE-modified group velocity at this value is approximately zero. As expected, the pulse has not moved after 1.5 units of time. In contrast, the same packet simulated using an eighth-order PSE approximation moves the correct distance, as Fig. 2b shows.

The use of the modified relationship between frequency and wavenumber to assess the error of PSE need not be limited to hyperbolic problems. The analysis is equally important in

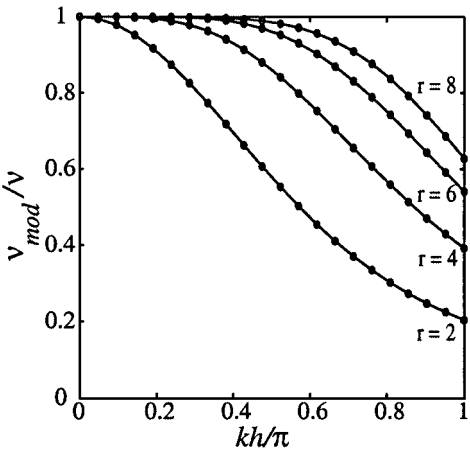

FIG. 3. Modified viscosity in applying PSE to diffusion equation with second-, fourth-, sixth-, and eighth-order kernels; $\kappa = 1.4$.

a diffusive context, revealing the extent to which numerical viscosity affects the components. Consider the one-dimensional diffusion equation,

$$\frac{\partial f}{\partial t} = \nu \frac{\partial^2 f}{\partial x^2}.$$

The exact relationship between frequency and wavenumber is $\omega(k) = -i\nu k^2$. Applying PSE to the spatial derivative results in the same modified wavenumber as for the wave equation (24). Alternatively, the modification can be viewed as affecting the viscosity. Expressing this new viscosity in terms of the kernel's integral moments, we have

$$\nu_{mod} = \nu \left(1 - \sum_{n=r/2+1}^{\infty} \frac{(\varepsilon k)^{2(n-1)}(-1)^{n-1}}{(2n)!} M_{2n} \right).$$

The discrete counterpart of this modified viscosity is plotted in Fig. 3 for the usual set of kernels. It is clear that high-wavenumber components are underdiffused, but that high-order-accurate kernels mitigate this discrepancy. A second-order-accurate kernel leads to too little diffusion for even well-resolved data, but eighth-order-accurate PSE performs much better.

It should be added that such a modification of the viscosity can actually be exploited. For inviscid simulations, Cottet [4] has shown that the numerical viscosity resulting from the mollifying of the velocity kernel in vortex methods—the mollifying leads to an error similar to that of PSE—can be tailored to derive an eddy viscosity model, which is essential for capturing the self-organizing of vorticity into large-scale structures from an initially chaotic field. Monaghan and Gingold [14] have used numerical viscosity to reduce the oscillations near shocks in SPH.

5. RESULTS

The tests described in this section are very simple, but they demonstrate fundamental characteristics of PSE that also arise when it is applied to more complex problems.

5.1. Rates of Convergence and Efficiency

The purpose of the set of tests described here is twofold: to demonstrate that the high-order-accurate PSE kernels derived in this paper do indeed lead to convergence at their designed rate, and to show that increasing the order of accuracy of a kernel leads to more efficient computation. The second derivative of the function,

$$f(x) = \frac{1}{\sqrt{\pi\sigma^2}} e^{-x^2/\sigma^2},$$

is used as the model for evaluation, with $\sigma = 0.05$. The derivative is approximated on a uniform grid of points on the domain $[-1/2, 1/2]$. The ratio of kernel radius to interparticle spacing, κ, is set at either 1.5 or 2. The discrete L_2 error between the exact derivative and its PSE approximation is computed for a variety of grid resolutions; kernels of second-, fourth, sixth-, and eighth-order accuracy are used. The results for $\kappa = 2$ are shown in Fig. 4. The error, ϵ, converges as expected for all four kernels: $\epsilon \propto h^r$ or, equivalently, $\epsilon \propto \varepsilon^r$.

A question we may ask is as follows: What is the minimum number of grid points needed to achieve some specified tolerance of error? The computational effort appears to be proportional to the square of the number of grid points, N^2, but with appropriate truncation of point-to-point interactions it can be made proportional to N. Thus, the minimum number of points required to reach a specific level of error is directly related to the *efficiency* of the kernel, a very useful metric. This information is readily available from Fig. 4 by choosing a level on the vertical axis and reading across to where the level intersects each kernel's convergence curve, then inverting the corresponding grid spacing to get N. For the level $\epsilon = 10^{-4}$, the results for each kernel are tabulated in Table I. Also displayed is the CPU time required to compute this derivative, on a SGI Octane with an R10000 processor. The second-order-accurate kernel requires a very large number of points to achieve the tolerance, while the fourth-order-accurate kernel needs only about 1/10 of this number, and the sixth- and eighth-order-accurate kernels require successively fewer.

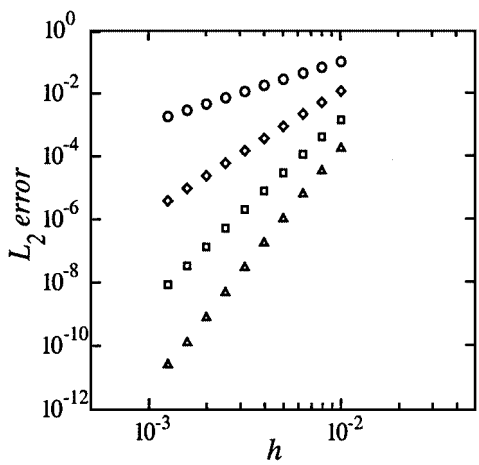

FIG. 4. Error in computing second derivative for several grid resolutions for kernels of varying order of accuracy. Order 2, ○; order 4, ◇; order 6, □; order 8, △.

TABLE I
Minimum Number of Particles to Achieve Error of 10^{-4} and Corresponding CPU Time

Order r	Minimum N	CPU time (s)
2	3440	4.28
4	354	0.0478
6	165	0.0114
8	111	0.00705

The data can be reduced to the following approximate relation:

$$\epsilon \approx 0.9(18\varepsilon)^r.$$

The appearance of a constant factor inside the parentheses may seem surprising. However, the error bound (10) contains the Sobolev norm of f, and it can be shown that this particular norm of the Gaussian is proportional to $1/\sigma^r$, so the error is bounded by $\epsilon \leq C'(\varepsilon/\sigma)^r$, where C' is another constant. In our tests $1/\sigma = 1/0.05 = 20$, so the results are consistent with the expected bound. This form of the error bound explains why the successive improvement in efficiency of each kernel over the previous one becomes less striking as r increases in Table I. The minimum number of grid points required to reach a fixed level of error is proportional to $(C'')^{1/r}$, where C'' is constant. Thus, past a certain point, increasing the order of accuracy of the kernel does not markedly improve the efficiency.

5.2. Wave Propagation Using Full-Space Kernels

The dispersive character of PSE when applied to hyperbolic problems was analyzed in Section 4. This character is exhibited in the following example involving a two-dimensional Gaussian pulse. Initially,

$$f(x, y) = \frac{1}{\pi\sigma^2} e^{-((x-x_0)^2+(y-y_0)^2)/\sigma^2},$$

which is allowed to convect at unit speed in a direction 54° relative to the x-axis, or the direction $\hat{\mathbf{c}} = (0.59,\ 0.81)$, on particles that are held fixed. This direction is chosen because it is not aligned with any grid symmetry. The initial configuration is shown in the upper plot in Fig. 5; the pulse radius σ is 0.1. The spatial derivative in the convective operator is approximated with PSE, with $\kappa = 1.8$, first using a second-order-accurate kernel and then an eighth-order-accurate one, on a uniform 51×51 grid. Thus, the core of the pulse is 11 particles in diameter. After 0.5 units of time, the pulse in the second-order case has significantly dispersed, but in the eighth-order case the pulse has not deformed and is located at the correct position.

5.3. Wave Propagation Using One-Sided Kernels

The previous example illustrated the use of PSE in convection problems when particle coverage is sufficiently isotropic about the kernel center. But this is not the case near the

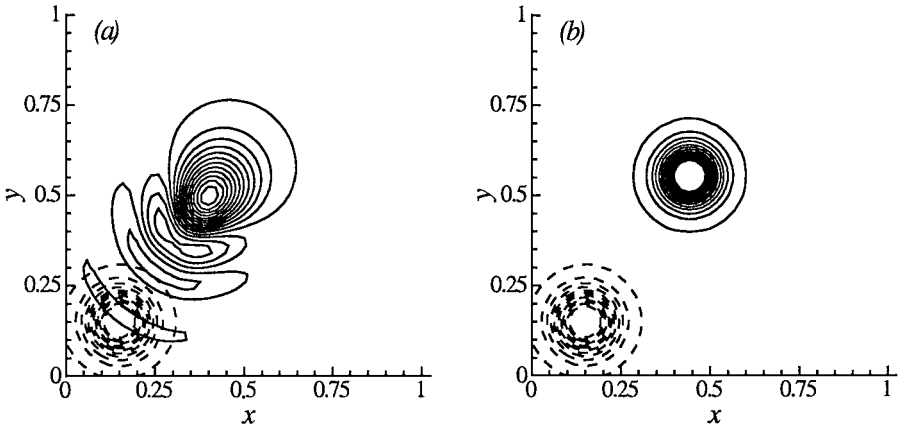

FIG. 5. Gaussian pulse convecting in direction $\hat{c} = (0.59,\ 0.81)$. At $t = 0$ (− − −) and $t = 0.5$ (———) using (a) a second-order kernel and (b) an eighth-order kernel.

edge of the computational domain, and one-sided kernels are useful in such circumstances. We solve the same problem here as in the previous example, situating the pulse initially at the center of the domain. Eventually the pulse travels to the upper right corner of the domain. Figure 6 demonstrates the instability that results from a waveform trying to pass out of a domain using an eighth-order-accurate full-space kernel. When the particles near

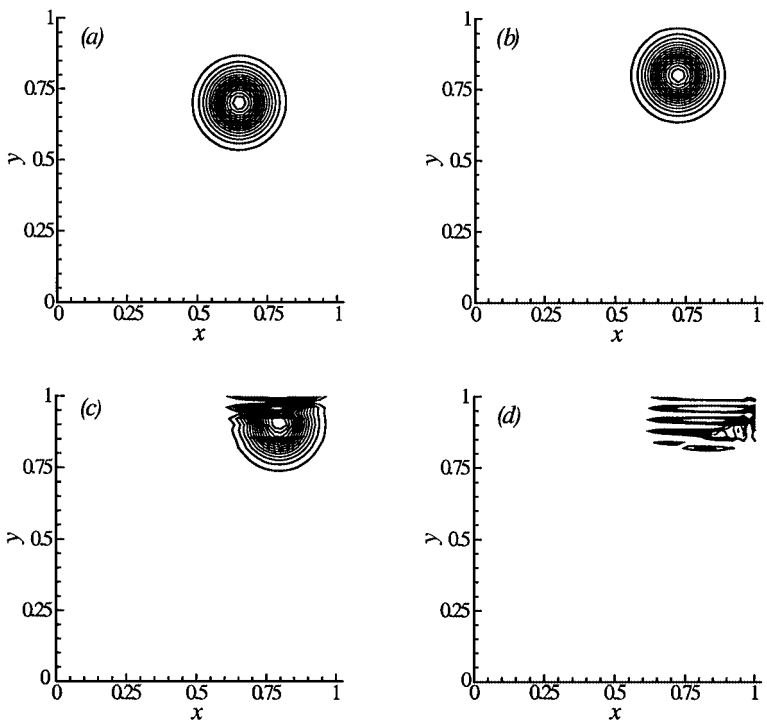

FIG. 6. Eighth-order full-space kernel in convection. At $t =$ (a) 0.25, (b) 0.375, (c) 0.5, and (d) 0.625.

the corner acquire strength, they lack neighbors downwind of the propagation direction with which to exchange their strength.

When a one-sided kernel is used, with the half-plane of integration chosen to coincide with the upwind direction, the instability of the full-space kernel is avoided, as demonstrated in Fig. 7. The kernel used here, which is third-order-accurate, only exchanges strength with particles on the upwind side of the pulse and thus has no difficulty near the boundary. Only slight dispersion of the pulse is apparent.

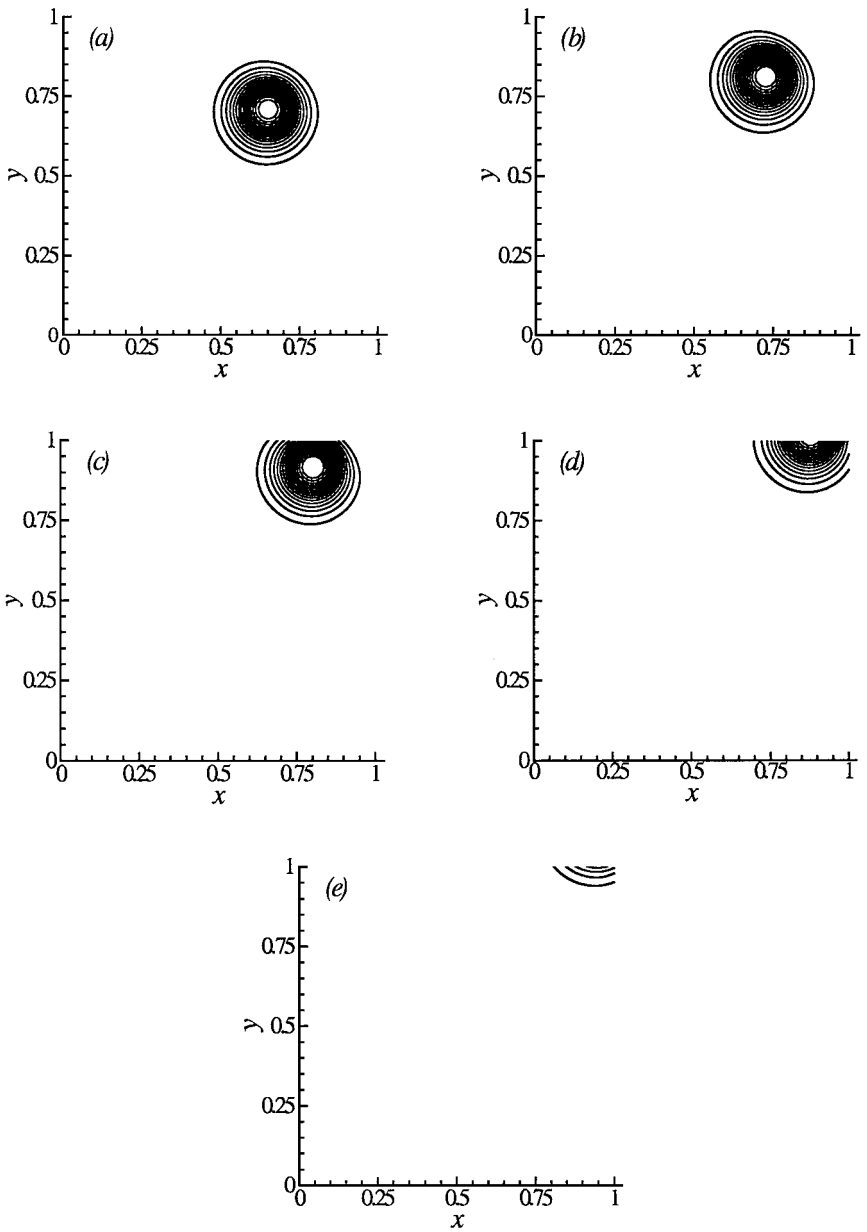

FIG. 7. Third-order one-sided kernel in convection, with one-sided integration plane aligned with upwind of propagation direction. At $t =$ (a) 0.25, (b) 0.375, (c) 0.5, (d) 0.625, and (e) 0.75.

5.4. Assessment of the Effects of Grid Distortion

The previous examples were all simulated on stationary grids, but a clear assessment of how PSE behaves when its quadrature points are dispersed by the flow map is also important. Consider the same Gaussian pulse, now convected with the velocity field $\mathbf{u}+\hat{\mathbf{c}}$, where $\hat{\mathbf{c}}=(0.59,\ 0.81)$, as before. Though not based on physics, this problem shares features that arise in physical phenomena. For instance, an acoustic wave that travels through a vortical region is convected by a velocity that is the sum of the fluid velocity and the local speed of sound. The equations governing the particles in the convecting frame are

$$\begin{aligned}\frac{d\tilde{f}_p}{dt} &= 0,\\ \frac{d\tilde{\mathbf{x}}_p}{dt} &= \mathbf{u}(\tilde{\mathbf{x}}_p(t))+\hat{\mathbf{c}},\\ \frac{d\tilde{V}_p}{dt} &= \operatorname{div}\mathbf{u}(\tilde{\mathbf{x}}_p(t))\tilde{V}_p(t).\end{aligned}$$

If initially $\tilde{\mathbf{x}}_p(0)=\boldsymbol{\xi}_p$, $\tilde{f}_p(0)=f(\boldsymbol{\xi}_p)$, and $\tilde{V}_p(0)=h^2$, then the solution is simply $\tilde{f}_p(t)=f(\boldsymbol{\xi}_p)$, $\tilde{\mathbf{x}}_p=\boldsymbol{\xi}_p+\hat{\mathbf{c}}t+\int_0^t\mathbf{u}(\tilde{\mathbf{x}}_p(\tau))\,d\tau$, and $\tilde{V}_p(t)=J(t;\boldsymbol{\xi}_p)h^2$, where $J(t;\boldsymbol{\xi})$ is the Jacobian of the flow map. However, this problem can also be solved by convecting the particles with velocity $\mathbf{u}$ and treating the convection by $\hat{\mathbf{c}}$ through a modification of the particle strengths. In this new frame,

$$\begin{aligned}\frac{df_p}{dt} &= -(\hat{\mathbf{c}}\cdot\nabla f)(\mathbf{x}_p(t)),\\ \frac{d\mathbf{x}_p}{dt} &= \mathbf{u}(\mathbf{x}_p(t)),\\ \frac{dV_p}{dt} &= \operatorname{div}\mathbf{u}(\mathbf{x}_p(t))V_p(t).\end{aligned}$$

As in the previous examples, the right-hand side term of the first equation is treated with PSE. We will separately consider two different types of velocity fields, $\mathbf{u}$: the first induced by a Gaussian-distributed vortex with circulation Γ_0 at the center of the domain, and the second induced by a Gaussian source of strength Q_0 at the same position. Both Gaussians have the same radius as the pulse, which is initially placed at (0.25, 0.25).

Under the vortex-induced velocity with $\Gamma_0=0.5$, the grid distortion after 0.25 units of time (or 25 time steps) is as shown in Fig. 8. The solution using eighth-order-accurate PSE with $\kappa=1.8$ is plotted with the exact solution at this time level in Fig. 9. The agreement is quite good, despite the dramatic stretching of the grid near the center of the domain. However, increasing the strength of the vortex to $\Gamma_0=0.85$ leads to breakup of the pulse as it passes through this straining region, as shown in Fig. 10a. Remeshing onto a uniform grid every 10 steps prevents the particles from becoming too dispersed, and Fig. 10b shows that the the exact solution is well approximated. Thus, PSE can withstand some distortion in the grid, but only to a degree, beyond which remeshing is necessary.

A source-induced velocity leads to dilatation of the particles, as shown in Fig. 11 for $Q_0=0.2$ at $t=0.35$, from which the obvious consequence is a loss of overlap of particles, as the kernel radius is held constant. Indeed, the pulse has become unstable at $t=0.35$, depicted in Fig. 12a. But remeshing every 10 steps prevents the particle spacing from

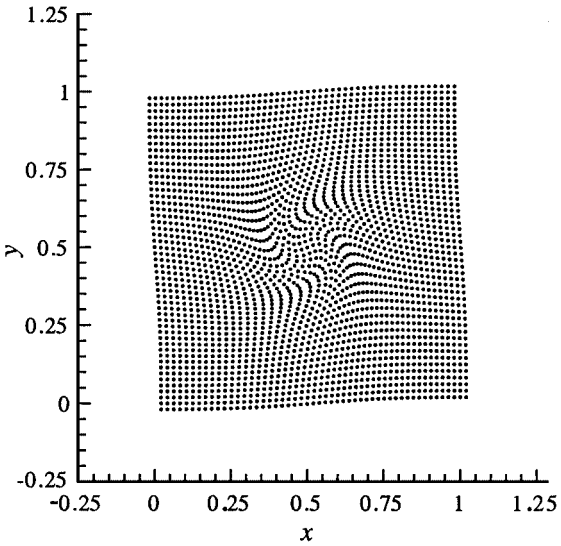

FIG. 8. Particle grid distorted by Gaussian vorticity field, $\Gamma_0 = 0.5$, at $t = 0.25$.

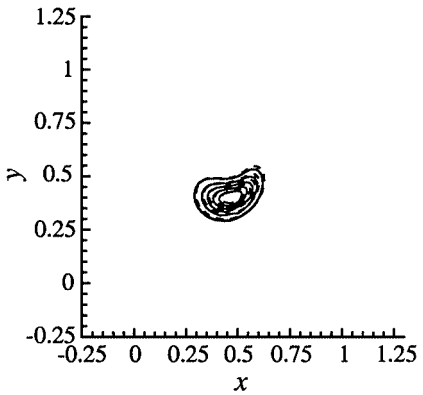

FIG. 9. Convection in $\hat{c} = (0.59,\ 0.81)$ plus Gaussian vorticity field, $\Gamma_0 = 0.5$, at $t = 0.25$. Using PSE, ——; exact, – – –.

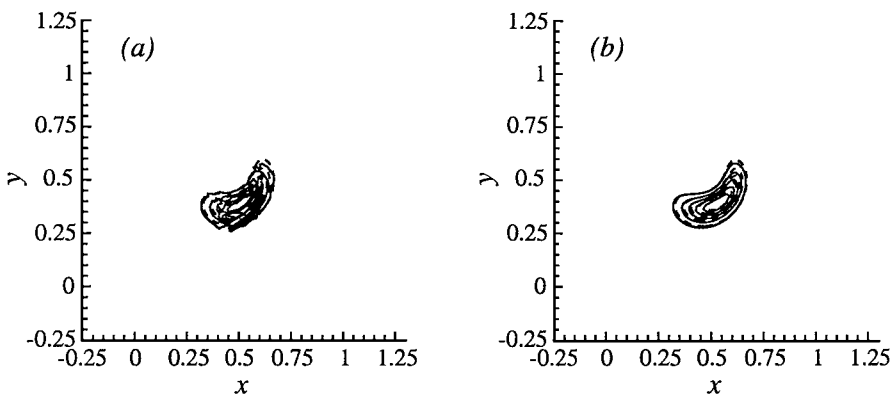

FIG. 10. Gaussian vorticity field, $\Gamma_0 = 0.85$, at $t = 0.25$. (a) Without remeshing, and (b) remeshing every 10 steps. Using PSE, ——; exact, – – –.

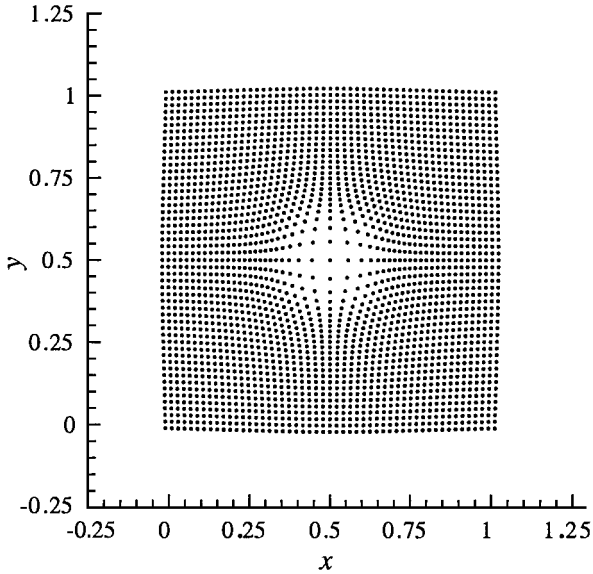

FIG. 11. Particle grid distorted by Gaussian source field, $Q_0 = 0.2$, at $t = 0.35$.

growing beyond ε, and so the pulse convects cleanly through the center of the domain, as shown in Fig. 12b.

If the particle grid undergoes dilatation without significant anisotropic straining, as in this example, then the need for remeshing may be delayed, or eliminated altogether. PSE can be adapted to account for variably sized particles, using a known mapping to a uniform grid, as shown by Cottet *et al.* [6], or by simply allowing variable kernel radius in the PSE operator, as described by Ploumhans and Winckelmans [15]. We demonstrate the latter method here. The local kernel radius is continuously adjusted to keep its ratio to the interparticle spacing near κ. To preserve the symmetry of the PSE operator, a mean of the squares of the kernel radii of particles p and q is used:

$$\varepsilon_{pq}^2 = \frac{\kappa^2}{2}(V_p(t) + V_q(t)).$$

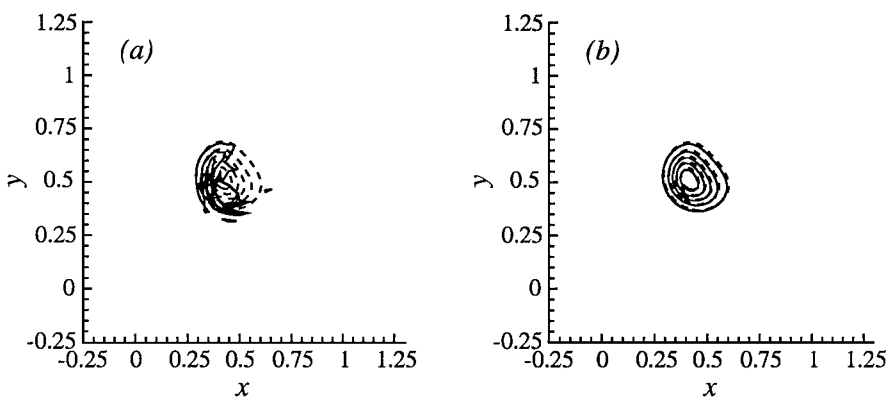

FIG. 12. Gaussian dilatation field, $Q_0 = 0.2$, at $t = 0.35$. (a) Without remeshing and (b) remeshing every 10 steps. Using PSE, ——; exact, – – –.

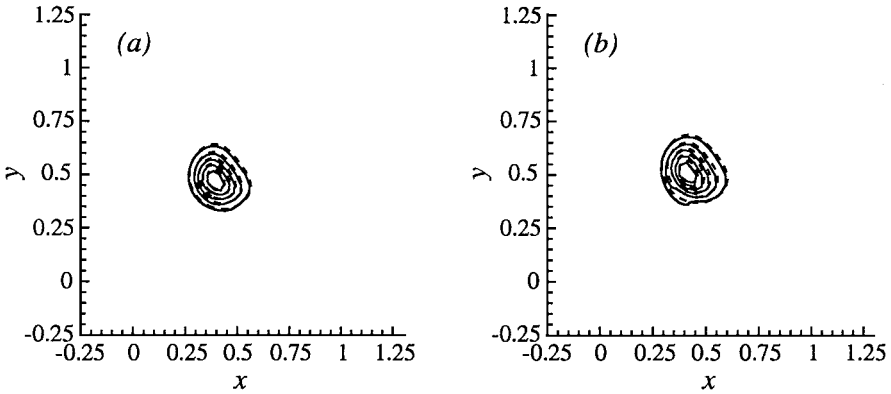

FIG. 13. Gaussian dilatation field, $Q_0 = 0.2$. (a) At $t = 0.30$ and (b) at $t = 0.35$. Variable-kernel-size PSE, ——; exact, – – –.

The results using this technique are shown in Fig. 13. In Fig. 13a, at $t = 0.30$, the pulse is passing through the region of expanded particles but still matches the exact solution quite well. The pulse at $t = 0.35$ exhibits some deformation, depicted in Fig. 13b. However, it is apparent that variable-kernel-size PSE has at least delayed the need for remeshing.

6. CONCLUSIONS

The deterministic method known as particle strength exchange for approximating the Laplacian by integral operators has been extended in the present work through the development of higher-order-accurate kernels for use in approximating arbitrary differential operators. These new kernels allow many new applications of PSE, particularly in wave propagation problems, but also in the baroclinic term in vortex particle methods for compressible flows [9] and other contexts not listed.

Use of PSE in the wave operator raises new questions, to which we have provided answers: What happens for waves (or other physical phenomena) near the periphery of particle coverage? Does a propagating pulse get dispersed by the PSE operator? For computing derivatives near the edge of the computational domain, we developed one-sided integral operators which only look inward for information. Such a treatment is used for enforcing a nonreflecting boundary condition by Eldredge *et al.* [9] and could be applied to wall-bounded flows as an alternative to the image treatment employed by Ploumhans and Winckelmans [15]. The dispersive character of PSE was explored and it was found that only high-order-accurate kernels should be used in these contexts. The efficiency of kernels was explored, and it was found that increasing the order of accuracy of the kernel improves the computational efficiency, but by an amount which decreases as the order increases. Finally, it was shown that on smoothly distorting grids PSE performs reasonably well, especially when kernels of variable size are employed, but that remeshing is ultimately essential for accuracy at long times.

APPENDIX: A LIST OF KERNELS

For reference, this appendix contains kernels of several orders of accuracy for application to first and second derivatives in one- and two-dimensional problems, in both full-space

and one-sided operators. As a shorthand, the kernel is expressed as

$$\eta^{(\alpha_1,\alpha_2,\ldots,\alpha_d)},$$

where the superscript indicates the α_1^{th} derivative in the x_1-direction, the α_2^{th} derivative in the x_2-direction, and so on.

One-Dimensional First Derivatives, Full Space

$$\eta^{(1)}(x) = \frac{x}{\sqrt{\pi}} e^{-x^2} \times \begin{cases} (-2), & \text{second order,} \\ (-5+2x^2), & \text{fourth order,} \\ \left(-\frac{35}{4}+7x^2-x^4\right), & \text{sixth order,} \\ \left(-\frac{105}{4}+\frac{63}{4}x^2-\frac{9}{2}x^4+\frac{1}{3}x^6\right), & \text{eighth order.} \end{cases}$$

One-Dimensional First Derivatives, Left Sided

$$\eta^{L,(1)}(x) = \frac{x}{\sqrt{\pi}} e^{-x^2} \times \begin{cases} (-4), & \text{first order,} \\ (-16+8x^2), & \text{second order,} \\ (-40+44x^2-8x^4), & \text{third order,} \\ \left(-80+144x^2-56x^4+\frac{16}{3}x^6\right), & \text{fourth order.} \end{cases}$$

Right-sided kernels are identical to the left-sided ones.

One-Dimensional Second Derivatives, Full Space

$$\eta^{(2)}(x) = \frac{1}{\sqrt{\pi}} e^{-x^2} \times \begin{cases} (4), & \text{second order,} \\ (10-4x^2), & \text{fourth order,} \\ \left(\frac{35}{2}-14x^2+2x^4\right), & \text{sixth order,} \\ \left(\frac{105}{4}-\frac{63}{2}x^2+9x^4-\frac{2}{3}x^6\right), & \text{eighth order.} \end{cases}$$

Two-Dimensional First Derivatives, Full Space

$$\eta^{(1,0)}(\mathbf{x}) = \frac{x_1}{\pi} e^{-|\mathbf{x}|^2} \times \begin{cases} (-2), & \text{second order,} \\ (-6+2|\mathbf{x}|^2), & \text{fourth order,} \\ (-12+8|\mathbf{x}|^2-|\mathbf{x}|^4), & \text{sixth order,} \\ \left(-20+20|\mathbf{x}|^2-5|\mathbf{x}|^4+\frac{1}{3}|\mathbf{x}|^6\right), & \text{eighth order.} \end{cases}$$

Note that the (0, 1) derivative is approximated using the same kernels with the x_1 factor replaced by x_2.

Two-Dimensional First Derivatives, Left Sided

$$\eta^{L,(1,0)}(\mathbf{x}) = \frac{x_1}{\pi} e^{-|\mathbf{x}|^2} \times \begin{cases} (-4), & \text{first order,} \\ (-20 + 8|\mathbf{x}|^2), & \text{second order,} \\ (-60 + 52|\mathbf{x}|^2 - 8|\mathbf{x}|^4), & \text{third order,} \\ \left(-140 + 196|\mathbf{x}|^2 - 64|\mathbf{x}|^4 + \frac{16}{3}|\mathbf{x}|^6\right), & \text{fourth order.} \end{cases}$$

Again, these kernels are identical to their right-sided counterparts, and they can be adapted for use in approximating the (0, 1) derivative by replacing x_1 by x_2.

Two-Dimensional Laplacian, Full Space

$$\eta^{\text{lap}}(\mathbf{x}) = \frac{1}{\pi} e^{-|\mathbf{x}|^2} \times \begin{cases} (4), & \text{second order,} \\ (12 - 4|\mathbf{x}|^2), & \text{fourth order,} \\ (24 - 16|\mathbf{x}|^2 + 2|\mathbf{x}|^4), & \text{sixth order,} \\ \left(40 - 40|\mathbf{x}|^2 + 10|\mathbf{x}|^4 - \frac{2}{3}|\mathbf{x}|^6\right), & \text{eighth order.} \end{cases}$$

ACKNOWLEDGMENTS

The first author gratefully acknowledges support under a NSF Graduate Research Fellowship. This research was supported in part by the National Science Foundation under Grant 9501349.

REFERENCES

1. J. P. Choquin and S. Huberson, Particles simulation of viscous flow, *Comput. Fluids* **17**, 397 (1989).
2. J. P. Choquin and B. Lucquin-Desreux, Accuracy of a deterministic particle method for Navier-Stokes equations, *Int. J. Numer. Methods Fluids* **8**, 1439 (1988).
3. R. Cortez, Convergence of high-order deterministic particle methods for the convection-diffusion equation, *Commun. Pure Appl. Math.* **50**, 1235 (1997).
4. G.-H. Cottet, Artificial viscosity models for vortex and particle methods, *J. Comput. Phys.* **127**, 299 (1996).
5. G.-H. Cottet and P. Koumoutsakos, *Vortex Methods: Theory and Practice* (Cambridge Univ. Press, Cambridge, MA, 2000).
6. G.-H. Cottet, P. Koumoutsakos, and M. L. O. Salihi, Vortex methods with spatially varying cores, *J. Comput. Phys.* **162**, 164 (2000).
7. G.-H. Cottet and S. Mas-Gallic, A particle method to solve the Navier-Stokes system, *Numer. Math.* **57**, 805 (1990).
8. P. Degond and S. Mas-Gallic, The weighted particle method for convection-diffusion equations. Part 1: The case of an isotropic viscosity, *Math. Comput.* **53**(188), 485 (1989).
9. J. D. Eldredge, T. Colonius, and A. Leonard, A vortex particle method for two-dimensional compressible flow, *J. Comput. Phys.* **179**, 371–399 (2002).
10. D. Fishelov, A new vortex scheme for viscous flows, *J. Comput. Phys.* **86**, 211 (1990).
11. R. A. Gingold and J. J. Monaghan, Smoothed particle hydrodynamics: Theory and application to non spherical stars, *Mon. Not. R. Astron. Soc.* **181**, 375 (1977).
12. P. Koumoutsakos, A. Leonard, and F. Pépin, Boundary conditions for viscous vortex methods, *J. Comput. Phys.* **113**, 52 (1994).

13. S. Mas-Gallic and P. A. Raviart, *Particle Approximation of Convection Diffusion Problems*, Technical Report R86013 (Laboratoire d'Analyse Numérique d I'Université Pierre et Marie Curie, 1986).
14. J. J. Monaghan and R. A. Gingold, Shock simulation by the particle method SPH, *J. Comput. Phys.* **52**, 374 (1983).
15. P. Ploumhans and G. S. Winckelmans, Vortex methods for high-resolution simulations of viscous flow past bluff bodies of general geometry, *J. Comput. Phys.* **165**, 354 (2000).
16. G. S. Winckelmans and A. Leonard, Contributions to vortex particle methods for the computation of three-dimensional incompressible unsteady flows, *J. Comput. Phys.* **109**, 247 (1993).